Innov Biosyst Bioeng, 2026, vol. 10, no. 1,
doi: 10.20535/ibb.2026.10.1.354760

Original article

APPLICATION OF IMAGE CORRELATION ANALYSIS TO DETECT CELL SENSITIVITY TO MAGNETIC FIELD

L.V. Marynchenko[1]*, V.V. Khokhlov[2], O.I. Nizhelska[3], V.O. Holub[4]

[1]Igor Sikorsky Kyiv Polytechnic Institute, Kyiv, Ukraine
[2]Non-Governmental Organization "Anil", Kyiv, Ukraine
[3]Institute of Applied Physics of NASU, Sumy, Ukraine
[4]Stockholm University, Stockholm, Sweden

Corresponding author: lolitamar@ukr.net

Received 4 January 2026; Accepted 27 February 2026

Background. The increase in technogenic electromagnetic load leaves open the question of its impact on living cells, which do not have a specific evolutionary mechanism for responding to such an environmental factor. Currently, there are not enough suitable tests that can detect the effects of weak electromagnetic fields. Visualization of morphological changes in cell structure by simple optical methods does not give results, therefore, an additional image processing mechanism may be useful.
Objective. To verify the suitability of the method of correlation analysis of microimages using the example of yeast cells dried in saline on a silicon substrate to detect the effect of a static magnetic field on the surface structure of cells that do not have defined mechanisms of sensitivity to it.
Methods. Digital microimages of drops of yeast suspension in saline, dried on silicon surfaces under the influence of a static magnetic field of 0.17 T and without the field, were analyzed by one of the fractal methods - the correlation dimension parameter was determined, which was based on the matrix of pixel brightness values.
Results. The suitability of the correlation analysis method for determining changes in the surface structure of yeast cells and sodium chloride crystals under the influence of a static magnetic field of 0.17 T during drying of the yeast suspension was shown: the correlation measurability index, which indicated the variability of the structures, increased for yeast cells, and decreased for NaCl crystals.
Conclusions. In the case of correlation dimension, unlike other dimensions, its calculation is carried out using brightness values, therefore, even those image elements that are almost indistinguishable to the eye are taken into account. That is why this method turned out to be sensitive to changes in the structure and relief of the yeast cell wall dried under the influence of a static magnetic field of 0.17 T, recording its complications, and also demonstrating a more homogeneous structure of the formed NaCl crystals.

Keywords: image processing; fractal analysis; correlation dimension; yeast cells; silicon; sodium chloride; crystallization; magnetic field; sensitivity; microscopy; surface properties; biotechnologies.

Introduction

The Earth's magnetic field (MF) is one of the factors that made the emergence and existence of life possible, therefore, living cells in the process of evolution must have mechanisms for its perception.

The influence of a magnetic field on the location of bacteria in a water droplet – "magnetotaxis" – was established by R. Blackmore [1]. Various microorganisms have been shown to be magnetosensitive. Such cells contain biogenic magnetic nanoparticles that form a chain with a sufficiently large dipole moment for the cell to orient itself along the lines of the Earth's magnetic field (~ 50 μT), which are directed approximately vertically in our latitudes. The system of orientation in space relative to the geomagnetic field may be the oldest on Earth, giving microorganisms an evolutionary advantage compared to chaotic movement. The mechanism of magnetotaxis appeared, presumably, to eliminate the toxicity of iron free radicals during the reduction/oxidation of Fe^{3+}/Fe^{2+}. Such organisms capable of producing magnetic biominerals were called "magnetogens" [2, 3].

But the vast majority of microorganisms, as well as other eukaryotic cells, do not have specific corresponding genes and an evolutionary mechanism for responding to a magnetic field. The natural geomagnetic field is not an important factor for them to survive in the corresponding environment. However, it has been more than a century since the man-made electromagnetic load on the environment began, and in recent years it has been rapidly increasing (orbiting communication satellites, wireless technologies, robotics, MRI devices, the development of military electronic warfare systems, etc.). Moreover, man-made magnetic fields exceed the geomagnetic field by orders of

magnitude [4–6]. The issue of the impact of weak (medium) electromagnetic fields (EMF) on living objects remains debatable. The fact that many studies conducted since the introduction of wireless communication have failed to confirm hypersensitivity to man-made electromagnetic fields as an environmental disease can be explained by a lack of understanding of the mechanisms, which has led to the development of inappropriate tests. Interdisciplinary research has proven that all life forms can respond to magnetic fields, for example, through cryptochrome proteins [6].

It is believed that static magnetic fields (SMF) do not interact with non-magnetic living cells, however, in [7] it was demonstrated that SMF with an induction of 8 to 300 mT can affect the cellular structures of human glioblastoma. SEM images revealed modification of cell shape, cell detachment, loss of villi and appearance of membrane roughness and bubbles. Under the influence of SMF, cells oriented differently. Atomic force microscopy showed a change in the texture of the membrane surfaces of cells exposed to SMF. It is known that external EMFs can alter the functioning of ion channels [8], which may result in changes in cell shape and membrane texture.

Typically, in biomedical research, such background factors are ignored unless they significantly alter the image. However, structural shifts that are imperceptible to the eye can have unpredictable biological consequences, possibly having an uncontrolled impact on the results of diagnostic tests, for example, using microchips, affecting the bioprinting (functioning) of bioprostheses, etc. Therefore, the detection of cell sensitivity to SMF and its biological interpretation, in particular through the improvement of cell imaging methods, is a relevant issue.

The accepted method for numerically describing a structure consisting of many similar elements, such as a cell culture or crystal growths, is fractal analysis [9]. In [10], an attempt was made to evaluate the ability of yeast, bacterial, and algae cells dried on a silicon substrate in SMF to self-organize using fractal analysis (box counting method). Regarding yeast suspended in saline, no obvious effect of SMF was detected, unlike yeast suspended in distilled water. It was concluded that this method has limitations on the dispersion of objects, the scale of the image, and also in cases where the effect of the solvent on the cells is stronger than the effect of the MF. Also, the droplet boundary, scale, weak contrast, and the image binarization procedure introduce errors into the calculations. Therefore, some of the image information is lost, and subtle differences in structure may not be recognized by this method.

In contrast, another subclass of fractal dimensions, correlation analysis, is based on an alternative approach to dimension definition. Correlation dimension is simpler and faster to compute than other fractal dimensions, such as Hausdorff dimension or box counting dimension.

Correlation dimension is a numerical measure of the chaotic behavior of a complex dynamical system, and its definition helps to distinguish dynamical systems whose behavior is driven by deterministic chaos from those systems that are completely driven by random noise. The first class of systems has a correlation dimension value that is a finite number, while the correlation dimension of the second class of systems is equal to infinity.

The higher the correlation dimension, the more filled with a set of points of a dynamical system is its space, and the more complex is the structure of the physical texture of this system. If we consider a strange attractor (a set of points in phase space that attracts the trajectories of a chaotic system, i.e. one that behaves unpredictably), then the correlation dimension shows how densely the trajectory of the attractor fills the region of space where it is defined [11–13].

The initial data for calculating the correlation dimension are most often time series. In the classical case of a strange attractor, for example, this is a numerical series that describes the dependence of one – x(t), two – x(t), y(t) or three – x(t), y(t), z(t) of its coordinates on time. To generalize, we can talk about the correlation dimension of a numerical series, each element of which reflects in numerical value a certain characteristic of the corresponding constituent element of the object under study. In the case of a digital grayscale image, as the simplest case, such a characteristic is the pixel brightness, and the constituent element, accordingly, is a pixel. By numbering the image pixels in a certain sequence and determining the brightness value for each pixel, we can obtain a numerical series that describes the image in the sense of calculating its correlation dimension.

Therefore, the application of correlation dimension calculation to the cells microimage analysis that do not have identified magnetic susceptibility mechanisms may have a significant advantage over the use of, for example, box counting dimension, as it involves the full use of the information contained in the image.

This work aim was to test the suitability of the correlation analysis method of microimages using the example of yeast cells dried in saline on a silicon surface to detect the effect of a static magnetic field on cells that do not have defined mechanisms of sensitivity to it.

Materials and Methods

Sample preparation

A suspension of washed *Saccharomyces cerevisiae* yeast cells in a sterile aqueous solution of 0.9% NaCl was applied with a microdispenser in 50 µl portions onto a polished, degreased surface of silicon wafers with a specific crystallographic plane. The substrates were of three types: n-silicon {111}, p-silicon

{111} and p-silicon {100}. The cell concentration in the suspension was ~ 10^6 cells/ml. The dimensions of the silicon wafers were sufficient to accommodate the suspension drops on them and their placement on the microscope stage. The drops were dried at room temperature, normal humidity, in an open volume, without forced ventilation. Control samples were dried freely at room temperature. Immediately after applying the drops, the test samples were placed in a static magnetic field of 0.17 T, with the magnetic induction lines perpendicular to the sample plane. The scheme of the installation for drying the sample is shown in Fig. 1.

After the drops dried, the formed textures on the silicon surface were examined and photographed using an AXIO Observer A1M Carl Zeiss metallographic microscope in reflected light at magnifications from x50 to x1000. The method is described in more detail in [10]. The obtained images were saved in jpeg format files with a resolution of 2560x1920 pixels identical for all samples. A total of 20 primary images were analyzed. In all cases, a lace-like structure of yeast cells and NaCl crystals was observed (Fig. 2). Individual cells and crystals were then analyzed from the primary images.

Calculation method

The obtained microimages were examined by correlation analysis using the following procedure.

1. The digital grayscale microimage was converted into the corresponding numerical series.

To do this, from the image contained in the raster graphic format jpeg file, using the ImageJ program [14], a text file with a matrix of pixel brightness values was obtained, which was converted into a text file containing a numerical series of image pixel brightness values using a script in the MathCad program [15]. In the same script, the image pixel brightness values were normalized to [0; 1] interval and reduced to a zero mean.

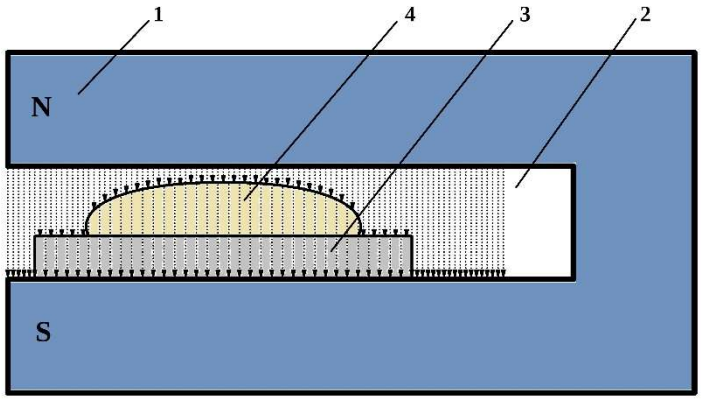

Figure 1. Scheme of the installation with a static magnetic field: 1 – permanent magnet; 2 – slit for placement samples; 3 – silicon wafer; 4 – drop of yeast suspension.

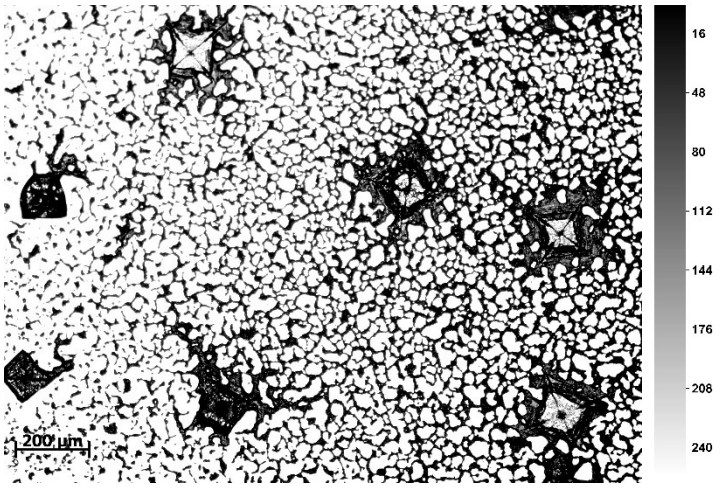

Figure 2. Example of a microimage (x50) of a dried drop of yeast suspension on a p-Si {100} silicon wafer (control) [10]; the grayscale contains the corresponding numerical intensity values.

2. The correlation dimension of the obtained numerical series was calculated using the d2 program from the TISEAN software package [16]. For convenience, the biopsyNLToolbox program [17] was used, which is a graphical interface for the d2 program. The d2 program result is a graph of the correlation dimension $D_2(\varepsilon, m)$ dependence on the neighborhood size ε and the embedding dimension m, an example of which for the microimage in Fig. 2 is shown in Fig. 3.

The embedding dimension (the dimension of the embedding space) is an integer m that determines the dimension of the space in which the correlation dimension is calculated using the Grassberger-Procacci algorithm. This is an m-dimensional space in which the correlation integral is calculated – the relative number of points pairs in a numerical series, separated from each other in each pair by a distance less than the neighborhood size ε. The function graph slope tangent of the fraction of the division of the natural logarithm of the correlation integral and the natural logarithm of the neighborhood size ε, provided that $\varepsilon \to 0$, is numerically equal to the correlation dimension $D2(\varepsilon, m)$ in this m-dimensional space.

In the default case, the correlation dimension graph consists of 10 separate graphs collapsed onto a single coordinate plane. Each of these separate graphs displays the dependence of the correlation dimension calculation value using the Grassberger-Procacci algorithm on the neighborhood size ε. Accordingly, for each of the ten graphs, the embedding dimension m value changes sequentially from 1 to 10. Three characteristic regions are distinguished in the graph. Region 1 is artifacts for small values of the neighborhood size ε. Region 3 is a region of divergence for large values of the neighborhood size ε, where the calculated value of the correlation dimension increases consistently as the embedding dimension m increases. These two regions do not contain any information about the correlation dimension value.

The actual correlation dimension value is determined in region 2, where the graphs reach a plateau and their convergence becomes apparent – a decreasing dependence on the value of the embedding dimension m.

But even at the plateau, the graph numerical data had too high a spread to allow the standard mean and standard error to be calculated by a generally accepted method. Therefore, given the classical definition of correlation dimension, it is most mathematically correct to calculate the correlation dimension as the mean of the two largest $D_2(\varepsilon, m)$ values for the embedding dimension m = 10 within the neighborhood size ε, provided that the convergence condition for these two values is met. If convergence was not observed at the entire ε = [0.07; 0.3] interval, then the two largest values were chosen at that subinterval within the neighborhood size ε = [0.07; 0.3] where the convergence condition was met. The error value was calculated in a standard way – as the difference between the previously calculated mean $D_2(\varepsilon, m)$ value and any of the two largest $D_2(\varepsilon, m)$ values. For the two-value case, there is no difference between simple (linear) and root mean square error.

For the highest results relevance, it is important, but not necessary, that all image samples have the same pixels number. The pixels number affects the sensitivity of the calculated value of the correlation dimension to the deterministic chaos component.

Results

As noted above, in the case of drying a drop of yeast cell suspension in saline on silicon substrates, a lacy pattern was observed in the microimages, which did not fundamentally differ from the control in the case of using 0.17 T induction value SMF (Fig. 1). Accordingly, the fractal dimension calculated by the box counting method also did not show significant differences (the fractal dimension D ranged from 1.77 to 1.78, and the lacunarity L ranged from 0.25 to 0.26) [10].

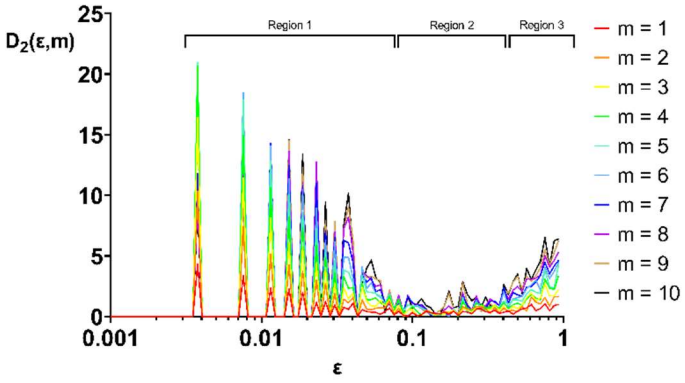

Figure 3. Correlation dimension $D_2(\varepsilon, m)$ graphs example for the microimage in Fig. 2 with the designation of characteristic regions.

Instead, the correlation dimension graphs for such microimages showed some differences. An example of microimages correlation dimension of yeast suspension droplets dried without and with SMF on p-Si {111} silicon substrates is shown in Fig. 4, 5, and in this pair, there is a distinct difference in correlation dimension at the highest visual similarity.

In particular, region 1 was present on all graphs without exception. Region 3 in the part of the graphs to which the graphs shown belong did not exhibit classical divergence. Therefore, it can be distinguished from region 2 – the plateau – either by the approximation of the D_2 values to zero, as in Fig. 5, or as in the case of Fig. 4: choose the plateau interval within the ε = [0.07; 0.3] characteristic limits.

The latter is mathematically correct, since it turned out that the plateau interval boundaries in those cases where it can be distinguished without problems depend only on the method of normalizing the initial data, and do not depend on the number of image pixels and the nature of the image itself. The method of initial data normalizing for all images is the same – they are normalized to [0; 1] interval and reduced to a zero mean.

Therefore, to detect the SMF effect on yeast cells (which do not have defined magnetic sensitivity mechanisms), the correlation dimension was calculated for microimages of yeast suspension drops dried on different silicon substrate types: n-silicon {111}, p-silicon {111} and p-silicon {100} under control conditions and under SMF exposure. For microimages at the same magnification within a pair, 4, 3, and 3 pairs of correlation dimension calculations were performed for each silicon type, respectively.

In all cases, after the SMF action, the D_2 dimension increased (Fig. 6).

In the microimages of dried drops of yeast suspension in saline, it was noticeable that the yeast and crystals formed a common structure (Fig. 2, 7 a, b). The microimage at higher magnification shows that yeast cells are more concentrated along the crystal edges (Fig. 7b) from its faces and edges, that is, in places where the crystal growth continues, and the growing NaCl crystal has set cubic symmetry in the space around it. However, the yeast cells actively interacted with each other and at a distance with the formed salt crystal, creating a lacy mesh, grouping, apparently, in areas with a higher salt concentration.

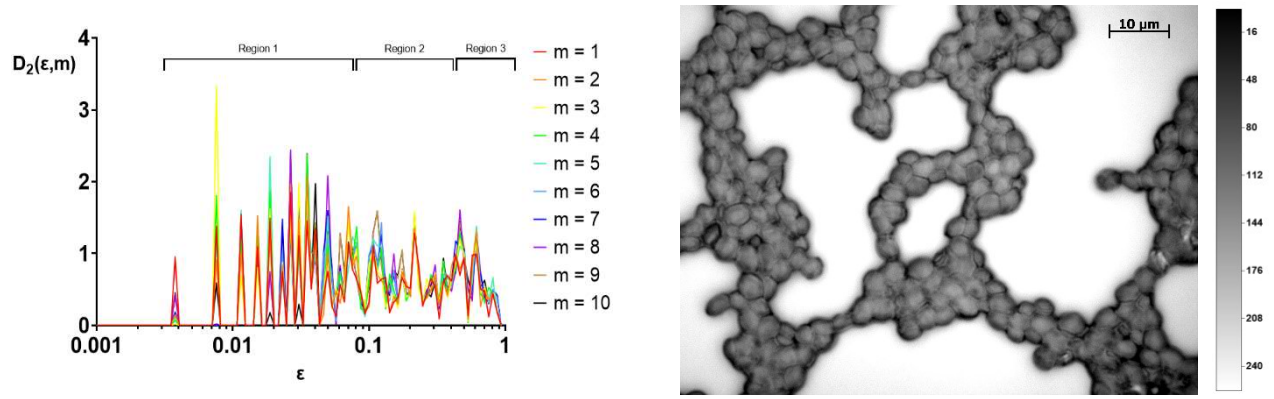

a) b)

Figure 4. a) The correlation dimension graph b) of the sample image on a p-Si {111} silicon wafer (x1000) without the SMF influence (control), D_2 = 1.56 ± 0.03; the grayscale contains the corresponding numerical intensity values.

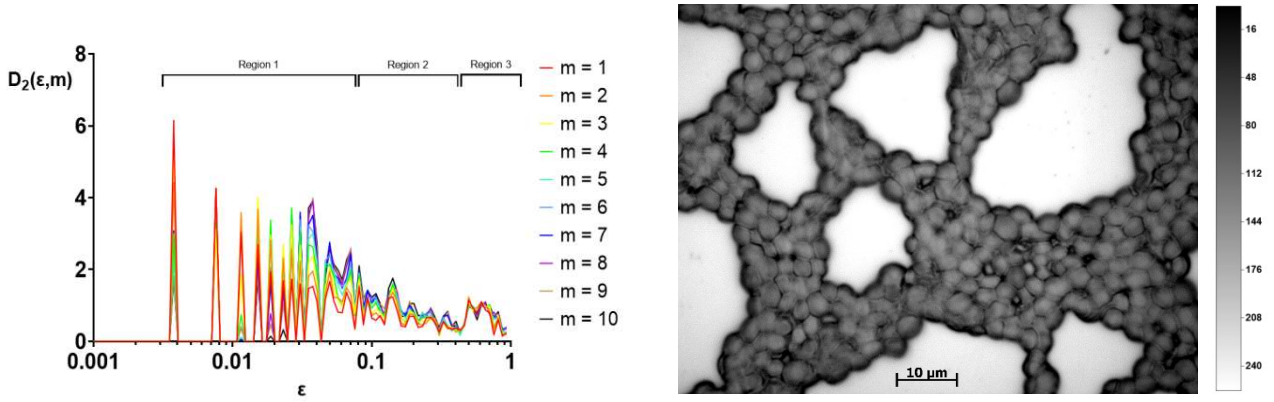

a) b)

Figure 5. a) The correlation dimension graph b) of the sample image on a p-Si {111} silicon wafer (x1000) with 0.17 T SMF influence, D_2 = 1.93 ± 0.17; the grayscale contains the corresponding numerical intensity values.

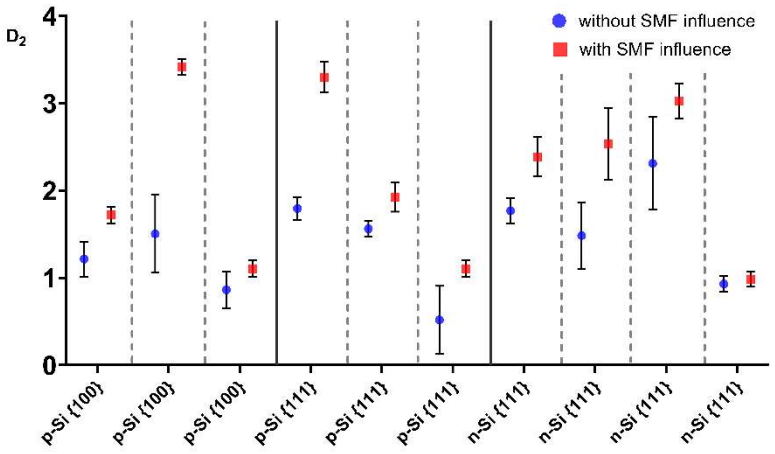

Figure 6. Correlation dimension values for microimages of yeast suspension dried on silicon substrates, calculated at the same magnification within a pair: p-Si {100} (3 image pairs), p-Si {111} (3 image pairs) and n-Si {111} (4 image pairs).

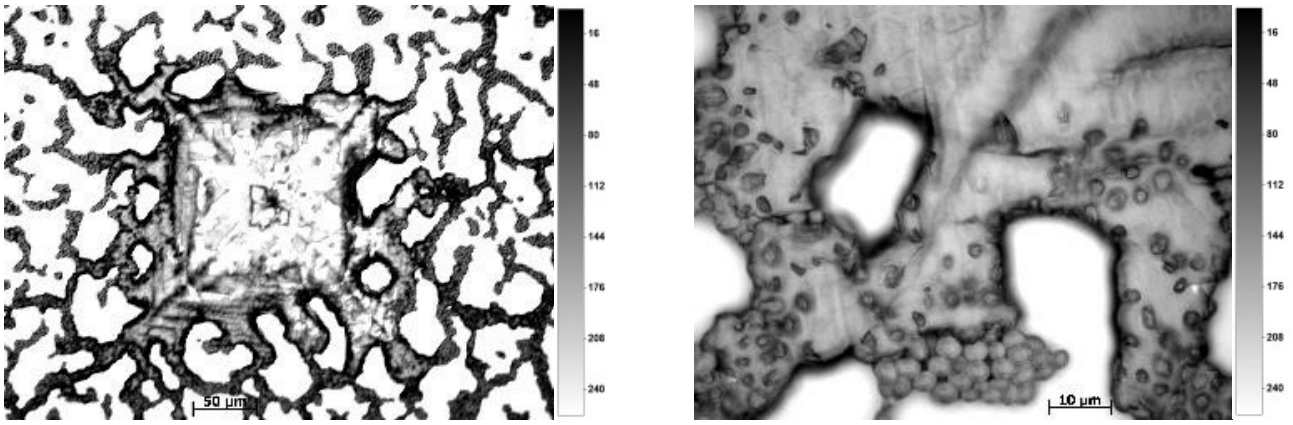

a) b)

Figure 7. The microimage examples of salt crystal samples of yeast suspension dried drop on p-Si {100} silicon wafer at different magnifications (control): a) x200, b) x1000 [10]; the grayscale contains the corresponding numerical intensity values.

To compare the SMF effect on the components of dried yeast suspension in saline, in addition to images of the entire structure (mesh) of the samples, an example of which is shown in Fig. 2, the correlation dimension was calculated separately for the samples – yeast cells and salt crystals in the control samples and under the SMF influence.

For this purpose, 10 individual cells with the same 150x150 pixels number were cut out from the x1000 images. Fig. 8 shows the the normal distribution of the correlation dimension for two samples of 10 individual cell images each. The normal distribution of the correlation dimension was calculated using *dnorm(x, μ, σ)* – a built-in Mathcad function.

Despite the fact that the correlation dimension values partially overlap, there is a noticeable D_2 shift towards an increase for cell samples that were exposed to SMF. The appearance distribution has not changed (Fig. 8).

From the literature data [18] it is known about the SMF effect on crystals; therefore, correlation analysis was applied to microimages of the formed NaCl crystals. The image for calculation was selected at a lower magnification (x50) because the formed salt crystals size was much larger than individual yeast cells.

To eliminate yeast cell clusters at the edges, a square mask was applied to the crystal image, the center of which coincided with the visible crystal center. The image size was on average 150x150 pixels, or 100x100 μm.

Fig. 9 shows individual crystal examples that were formed after the suspension dried in control samples and under the SMF influence.

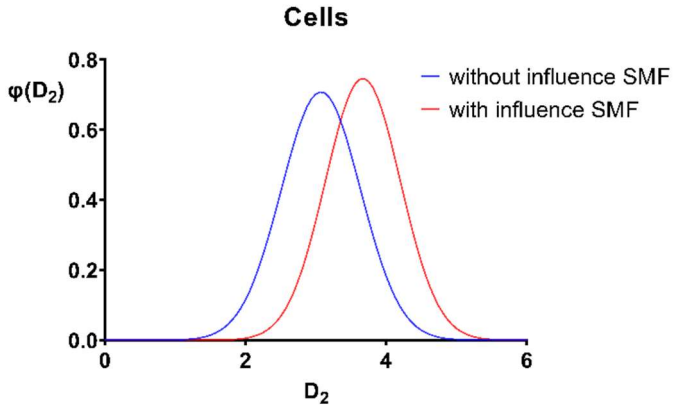

Figure 8. The normal distribution of the correlation dimension for two samples of 10 individual cell images (x1000) of suspension dried on different silicon types.

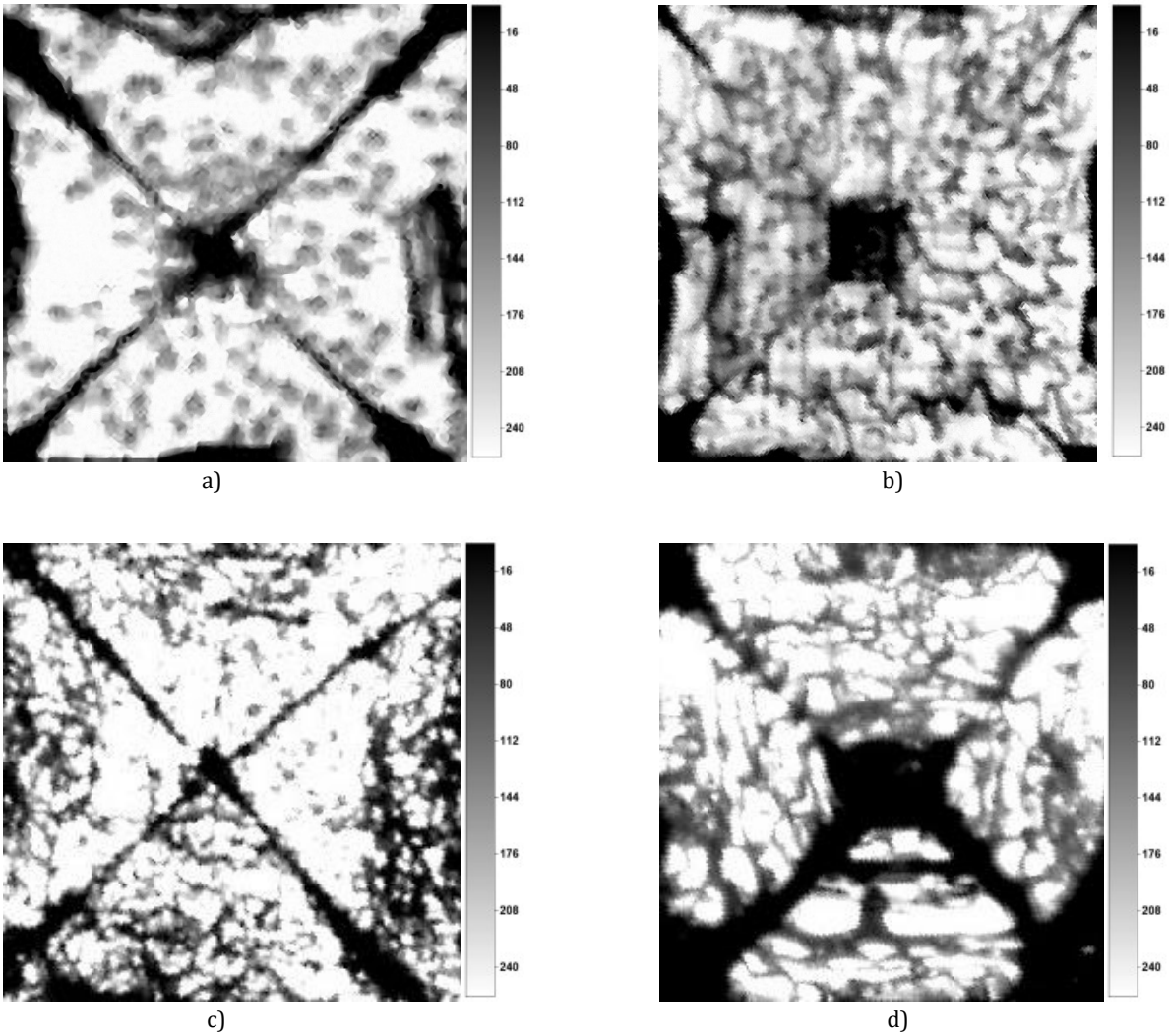

Figure 9. The image examples of individual NaCl crystals cut from x50 micrographs and calculated correlation dimension parameter D_2: a) (D_2 = 3.06 ± 0.37), b) (D_2 = 4.85 ± 0.63) – control; c) (D_2 = 1.58 ± 0.03), d) (D_2 = 1.18 ± 0.32) – under the SMF influence; the grayscale contains the corresponding numerical intensity values.

Fig. 10 presents the normal distribution of the correlation dimension for two samples of 5 individual NaCl crystal images (x50) each, which were formed without SMF influence (control), and under 0.17 T SMF influence.

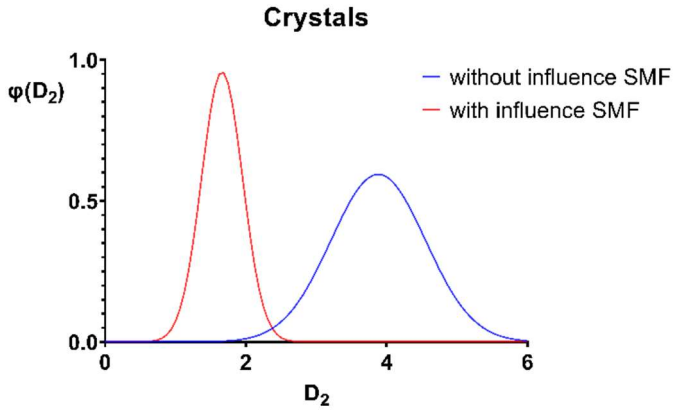

Figure 10. The normal distribution of the correlation dimension for two samples of 5 individual crystal images (x50) of suspension dried on different silicon types.

The obtained D_2 values for crystals exposed to SMF were lower than in control samples (unlike D_2 for yeast cells). Also, the normal distribution of the correlation dimension for crystals under the SMF action showed a shift opposite to the shift for yeast cells.

Discussion

The study design belongs to the correlational type, namely the "case-control" subtype. Since we previously observed the SMF effect on the cell membranes preservation after drying of yeast suspension, we assumed that changes in the microstructure still occur, and they can be detected using another method of fractal analysis, which takes into account not the contours of the image, like the *box counting* method, but the brightness of the pixels in it. This method (correlation analysis) proved to be suitable for identifying differences between individual comparable photos and for numerically evaluating such differences. The calculation of the correlation dimension value was based on the matrix obtained from the brightness of pixels in images with the same magnification: the changes that occurred in a dried yeast cells suspension under the 0.17 T SMF influence were shown (Fig. 6). The droplets dried on different types of silicon wafers, which are used as semiconductors both for converting solar energy into electricity and in microchips for diagnostic purposes. For all types of silicon studied, the value of the correlation dimension increased, although fractal analysis using the *box counting* method did not reveal any changes.

To interpret the results, magnified microimages of individual cells and individual salt crystals were analyzed. Correlation dimension D_2 calculation for images of control samples and those exposed to SMF was carried out for two data sets: yeast cells and sodium chloride crystals. Based on the results of calculating for cells and salt crystals that correspond to each other in terms of similarity and number of pixels, a normal distribution of the correlation dimension was constructed separately for cells and crystals (Fig. 9 and 10). Since in the case of yeast cells, only the surface of the cells is visible in the microimages, not their contents, it is quite reasonable to assume that changes in the structure and relief of the cell surface occurred under the influence of the magnetic field, which was revealed by the correlation analysis method. Changes were also assessed for individual, more transparent, salt crystals that formed during the drying of the drop, which indicates the suitability of the correlation analysis method for detecting sensitivity to EMF exposure not only in living objects.

The correlation analysis presented data of microimages of yeast suspension in physiological solution, dried on different silicon substrates without and under SMF influence, indicate differences in the D_2 calculated parameter values (Fig. 6), in contrast to the *box counting* method, which did not show changes in the parameters of fractal dimension D and lacunarity L [10]. As can be seen, the correlation dimension under SMF influence increased for all samples, although the type of silicon wafer on which the suspension dried may also affect the D_2 parameter.

According to the definitions contained in the Grassberger-Procacci algorithm description, the key concepts for the possibility of using graphs numerical data to calculate a specific value of the image correlation dimension are: 1) reaching graphs plateau; 2) the convergence presence – in the case of a sequential increase in the embedding dimension m from 1 to 10, the graph dependence on its value becomes less and less with each subsequent step of the embedding dimension m.

However, as can be seen from the graphs given (Fig. 3, 4), their appearance does not have such characteristic regions as shown in Fig. 3. In the general case, the correlation dimension increased with increasing embedding dimension m and changing the neighborhood size ε for all samples only in region 1. In region 3, for some samples, the correlation dimension increased with increasing embedding dimension m

and the neighborhood size ε as well, for another samples part it decreased to zero with increasing the neighborhood size ε, and in another samples part, the D_2 value remained at the plateau level, similar to region 2.

Therefore, it is possible to distinguish region 3 from region 2 – the plateau – either by approaching of the D_2 values of to zero, or by choosing the plateau interval within the specified characteristic ε = [0.07; 0.3] limits. As noted above, the plateau interval boundaries in those cases where it can be easily distinguished visually depend only on the method of normalizing the initial data, and therefore do not depend on the image pixels number and the nature of the image itself.

Since previously for calculations the pixel brightness data from the image were normalized to [0; 1] interval and reduced to zero mean, it can be expected that the plateau in all graphs will be contained in the same value limits of neighborhood size ε from 0.07 to 0.3. Therefore, the relevant data for further calculation of the image correlation dimension value are in region 2.

According to the correlation dimension classical definition, its value is the consecutive counts upper limit under the condition of a fixed value of the neighborhood size ε in the case of a consecutive increase in the embedding dimension m. It follows that, if there is convergence, for calculating of the correlation dimension for a given neighborhood size ε, one can choose the numerical data of only one graph out of ten for the embedding dimension m = 10.

Since each image, in addition to the actual study objects, also contains random noise caused by various reasons, it is necessary to note how its presence affects the results of calculating the correlation dimension. From a mathematical point of view, random noise is an image additive component and, since the same conditions and the same equipment cause the same random noise and the same share of it, in the correlation dimension value it represents a certain constant term. Therefore, if the images are obtained under the same conditions and on the same equipment, then random noise will increase the correlation dimension value equally on all samples and will not be significant for the comparison purpose. It should be noted that the droplet edge or scale bar are linear structures and do not have the property of very high correlation dimension values such as random noise, so they do not significantly affect the calculation results.

Similar remarks are quite valid regarding the impact on the results of calculating the correlation dimension of the losses and artifacts inherent in JPEG raster graphic format files during encoding. From a mathematical point of view, these losses and artifacts during encoding also represent an additive component of the image. Since their size and nature depend only on the JPEG encoding software algorithm, they are identical for images obtained on the same equipment. Therefore, in the meaning of the correlation dimension, they, like random noise, will represent a certain constant term. From this we can conclude that for the comparison purpose, these losses and artifacts will not affect the result.

Since on the presented microimages obtained with a metallographic microscope only be seen the general lacy pattern of a dried drop of yeast suspension in saline and the surface of yeast cells, it is logical to assume that the differences revealed by correlation analysis may relate specifically to the structure of the cell surface. Thus, the correlation analysis method can reveal significant changes just in the structure of cell shells. In the case of a yeast suspension in saline solution exposed to a static magnetic field (SMF) of 0.17 T during drying, such changes are probably cannot be significant enough, as demonstrated in Fig. 8.

This assumption is supported by other studies testifying a substantial biological impact of magnetic fields (MF) on ion channel permeability [19]. Such effects have been manifested, for example, in the enhanced adsorption of chemotherapeutic drugs due to the formation of nanosized pores in the cell membrane [20]. In particular, an enhanced the *in vitro* action of paclitaxel against human leukemia K562 cells under exposure to an SMF of 8.8 mT has been reported [21]. Disruption of ion channel function under external EMF can alter intracellular ion concentrations, thereby disturbing the electrochemical balance of the cell [8]. Therefore, modulation of ion channel activity is a plausible mechanistic pathway underlying the observed change in cell shape and membrane texture.

Visual inspection under optical microscopy revealed that the effect of the SMF was detectable only when the field was applied during the drying process of the suspension – that is, while convection, evaporation, salt crystallization, osmotic processes at the cell membrane, and adhesion to the substrate were actively occurring within the droplet. If the drying process had been completed in the absence of SMF exposure and the associated physicochemical dynamics had ceased, no subsequent changes in the cell shape or in the structure of the dried saline samples were observed after placement in the SMF [10].

It is clear that in a hypotonic environment, specifically in samples of cells suspended in distilled water, cell shells rupture was observed with subsequent pronounced cell degradation. However, samples of the same yeast suspension that were dried under the exposure to a SMF remained virtually intact after more than one year of observation, and their shape did not change. In contrast, in saline solution, which is isotonic for the cells, the optically visible shape of the yeast cells remained stable regardless of SMF exposure. Nevertheless, this does not preclude the presence of micro-scale alterations in the relief or structura

organization of the cell shells that are not detectable by optical microscopy [10].

These micro-scale alterations were identified in our study as an increase in pixel intensity variability in the analyzed images compared with control micrographs. In contrast to the *box-counting* method, the correlation dimension parameter increased even in cases where no visible changes were detectable under optical microscopy. We attribute the structural modifications of the cell shell revealed by correlation analysis to the influence of the SMF on the ion channel activity, alterations in the permeability of the chitinous/cellulosic cell wall, changes in hydrophobic/hydrophilic properties, and enhanced adsorption of substances onto the cell surface, which may contribute to its stabilization.

As previously noted, images acquired at ×50 magnification (Fig. 9) were selected for the analysis of the correlation dimension of individual salt crystals. For accurate calculation, it was essential that each image contained a single crystal in its entirety as an independent, integral structure, without adjacent cells, the presence of which in large numbers could distort the computational results. To address this, cropped images of individual crystals were rotated around an axis passing through the crystal center to ensure that the rectangular region of interest included only the crystal itself and excluded surrounding cells clustered in its vicinity.

As shown in Fig. 10, the correlation dimension D_2 for individual crystals formed under SMF exposure during drying of the yeast suspension in saline also changed, with effects more pronounced than those observed for yeast cells. For cells, SMF exposure resulted in an increase in correlation dimension while preserving the distribution half-width, whereas for salt crystals the opposite effect was observed: a decrease in correlation dimension accompanied by narrowing of the distribution.

The observed variations in D_2 confirm the influence of SMF on NaCl crystallization reported by other researchers. For example, study [18] demonstrated that a SMF of 55 ± 3 mT altered the growth rate of diamagnetic sodium chlorate ($NaClO_3$) crystals differently along distinct crystallographic directions, resulting in lattice parameters differing compared to control samples. Changes occurring at the surface of the growing crystal under SMF exposure are considered the key factor, which likely contributed to the observed variation in correlation dimension index.

For NaCl crystals formed under SMF exposure, in contrast to yeast cells, narrowing of the normal distribution and reduction of fine structural details were observed. In other words, crystals formed in a magnetic field become more homogeneous and structurally "cleaner," with smoother facets. Study [22], using theoretical modeling, analyzed the influence of a static magnetic field of 55 ± 3 mT on the growth kinetics of sodium chlorate crystal faces within a supersaturation range of 0.89–1.78% and demonstrated that crystal growth occurred via a complex dislocation source mechanism. Suppression of dislocation motion under SMF exposure may enhance crystal surface purity. As shown in Figs. 6 and 8, control samples exhibited greater incorporation of yeast cells into growing crystals, likely due to adhesion to growth surfaces, whereas crystals formed under SMF exposure were significantly cleaner. It can be assumed that such crystals contained fewer dislocations available for cell attachment. These findings are consistent with results reported in [23], where a magnetic-field-induced dislocation pinning effect was observed on the surface of single-crystal silicon under a magnetic field of 0.33 T. Therefore, the type of silicon substrate may also influence sodium chloride crystallization.

It should be noted that the informational value of images for correlation analysis increases with microscope magnification. Considering the origins of correlation analysis – the study of strange attractor, its dimension increases with increasing dynamical chaos; and if the dimension is limited from 1 to 3, this corresponds to an increase in the branching of the trajectories of the strange attractor. When applied to yeast cell surface structure, this interpretation suggests that SMF exposure may increase variability in surface relief, pore number and size, and receptor structural organization. For crystal images obtained at different magnifications, the shift of the normal distribution under SMF exposure would likely vary in magnitude; however, the direction of the shift – opposite to that observed for cells – would remain unchanged.

The correlation analysis method has certain limitations. Reliable results are obtained only when processing images with sufficient resolution and appropriate object scale. The minimum resolution expected to yield meaningful results is approximately 64 × 64 pixels. A further limitation concerns scale: the analyzed object or objects must occupy more than 25% of the original image area. These objects correspond to image regions, which capable of revealing potential differences induced by the investigated external factors. When multiple objects are present, the minimum resolution requirement applies to each individually.

Beyond demonstrating the sensitivity of yeast cells to SMF exposure, under conditions of increasing electromagnetic environmental load, correlation analysis may enable the development of methods for detecting extraneous EMF effects including impacts on soil microorganisms. Changes in the D_2 parameter of selected samples may therefore serve as indicators (test parameters) of external magnetic field exposure. In such systems, living cells may function as sensitive elements, whose images are captured by a photosen-

sor and processed by a microcontroller for calculation and signal indication. In medical and biotechnological applications, correlation analysis may also prove useful for processing color images, as modern software packages allow computation using multiple numerical series (e.g., up to four in TISEAN), corresponding to the red (R), green (G), and blue (B) image channels. Furthermore, comparison between artificial composite structures produced by 3D printing and healthy biological tissues may enable development of printing algorithms capable of generating materials closely resembling natural structures [24]. Another promising direction involves evaluating the influence of magnetostatic fields in the range of 1–10 mT on soil bioremediation processes [25]. Correlation analysis enables separation of SMF interactions with mineral components (aqueous solutions) and soil microorganisms and may assist in identifying strains resistant to technogenic stress for the preparation of dried microbial formulations used in soil restoration.

Conclusions

The suitability of the method of correlation analysis of digital images for determining the sensitivity of a suspension of yeast cells to the action of a static magnetic field is shown in cases where *box counting* analysis of these microimages did not reveal significant differences.

For yeast suspensions dried on three types of silicon substrates – n-silicon {111}, p-silicon {111} and p-silicon {100} – the effect of SMF led to an increase in the correlation dimension D_2, on average, from 3.07 to 3.67, and for salt crystals – on the contrary, to a decrease in D_2, on average, from 3.88 to 1.66. The increase in the correlation dimension is mathematically related to an increase in the variability in pixel brightness, and physically – to a change in the structure of the cell wall and its relief.

When exposed to a magnetic field, the correlation analysis method can detect subtle changes in the microstructure of cell shells, namely their permeability, as well as changes in the structure of NaCl crystals, namely their homogeneity.

Interests disclosure

The authors declare that there are no conflicts of interests

Acknowledgements

The authors express their gratitude to Alla Kuryliuk (PhD, Assistance Professor) from the Department of Metal Physics at Kyiv National University named after Taras Shevchenko, for providing samples of silicon and assistance in conducting experiments.

References

[1] Blakemore R. Magnetotactic bacteria. Science. 1975;190:377-379. DOI:10.1126/science.170679

[2] Lefèvre CT, Bazylinski DA. Ecology, diversity, and evolution of magnetotactic bacteria. Microbiol Mol Biol Rev. 2013;77(3):497-526. DOI:10.1128/MMBR.00021-13

[3] Islam T, Peng C, Ali I. Morphological and cellular diversity of magnetotactic bacteria: A review. J Basic Microbiol. 2018;58(5):378-389. DOI:10.1002/jobm.201700383

[4] Hedendahl L, Carlberg M, Hardell L. Electromagnetic hypersensitivity—an increasing challenge to the medical profession. Rev Environ Health. 2015;30(4):209-215. DOI:10.1515/reveh-2015-0012

[5] Weller SG, McCredden JE, Leach V, Chu C, Lam AK. A scoping review and evidence map of radiofrequency field exposure and genotoxicity: assessing in vivo, in vitro, and epidemiological data. Front Public Health. 2025;13:1613353. DOI:10.3389/fpubh.2025.1613353

[6] Henshaw DL, Philips A. A mechanistic understanding of human magnetoreception validates the phenomenon of electromagnetic hypersensitivity (EHS). Int J Radiat Biol. 2025;101(2):186-204. DOI:10.1080/09553002.2024.2435329

[7] Teodori L, Albertini MC, Uguccioni F, Falcieri E, Rocchi MB, Battistelli M, et al. Static magnetic fields affect cell size, shape, orientation, and membrane surface of human glioblastoma cells. Cytometry A. 2006;69(2):75-85. DOI:10.1002/cyto.a.20208

[8] Panagopoulos DJ, Karabarbounis A, Yakymenko I, Chrousos GP. Human made electromagnetic fields: Ion forced oscillation and voltage gated ion channel dysfunction, oxidative stress and DNA damage (Review). Int J Oncol. 2021;59(5):92. DOI:10.3892/ijo.2021.5272

[9] Mandelbrot BB. The fractal geometry of nature. New York: W.H. Freeman & Company; 1999. 468 p.

[10] Marynchenko LV, Nizhelska OI, Shirinyan AS, Gorchakova NO. Evaluation the interaction between silicon surface and microorganisms in various solvents under the influence of a static magnetic field using fractal analysis. Innov Biosyst Bioeng. 2024;8(2):69-84. DOI:10.20535/ibb.2024.8.2.297364

[11] Grassberger P, Procaccia I. Characterization of strange attractors. Phys Rev Lett. 1983;50(5):346-349. DOI:10.1103/PhysRevLett.50.346

[12] Grassberger P. Generalized dimensions of strange attractors. Phys Lett A. 1983;97(6):227-230. DOI:10.1016/0375-9601(83)90753-3

[13] Grassberger P, Procaccia I. Dimensions and entropies of strange attractors from a fluctuating dynamics approach. Physica D. 1984;13(1-2):34-54. DOI:10.1016/0167-2789(84)90269-0

[14] ImageJ [Internet]. Available from: https://imagej.net/ij/

[15] Mathcad [Internet]. Available from: https://www.mathcad.com/en/

[16] TISEAN 3.0.1 software [Internet]. Available from: https://www.pks.mpg.de/tisean/Tisean_3.0.1/index.html

[17] BioPsyNL Toolbox [Internet]. Available from: https://biopsynltoolbox.sourceforge.net/
[18] Milojević MM, Vučetić BM, Maksimović BZ, Klisurić OR, Mitrović MM, Žekić A. Influence of a static magnetic field on the ⟨100⟩ growth rates of sodium chlorate crystals from aqueous solution. ACS Omega. 2022;7:47701-47708. DOI:10.1021/acsomega.2c04790
[19] Nittby H, Persson BR, Salford LG, Brun A, Eberhardt JL, Malmgren L. Increased blood–brain barrier permeability in mammalian brain 7 days after exposure to the radiation from a GSM-900 mobile phone. Pathophysiology. 2009. DOI:10.1016/j.pathophys.2009.01.001
[20] Xu A, Wang Q, Lv X, Lin T. Progressive study on the non-thermal effects of magnetic field therapy in oncology. Front Oncol. 2021;11:638146. DOI:10.3389/fonc.2021.638146
[21] Sun RG, Chen WF, Qi H, Zhang K, Bu T, Liu Y, et al. Biologic effects of static magnetic fields and paclitaxel on K562 human leukemia cells. Gen Physiol Biophys. 2012;31:1-10. DOI:10.4149/gpb_2012_002
[22] Milojević MM, Žekić A, Maksimović BZ, Vučetić BM, Mitrović MM. Influence of magnetic field on growth kinetics of sodium chlorate crystals from aqueous solution. J Cryst Growth. 2024;642:127776. DOI:10.1016/j.jcrysgro.2024.127776
[23] Krit O, Shirinyan A, Marynchenko L, Nizhelska O. Assessment of changes in the texture of the silicon surface under the influence of a magnetic field and high-temperature plastic deformation using fractal analysis. Him Fiz Tehnol Poverhni. 2025;16:339-347.
[24] Rosellini E, Cascone MG, Guidi L, Schubert DW, Roether JA, Boccaccini AR. Mending a broken heart by biomimetic 3D printed natural biomaterial-based cardiac patches: A review. Front Bioeng Biotechnol. 2023;11:1254739. DOI:10.3389/fbioe.2023.1254739
[25] Beretta G, Mastorgio AF, Pedrali L, Saponaro S, Sezenna E. The effects of electric, magnetic and electromagnetic fields on microorganisms in the perspective of bioremediation. Rev Environ Sci Biotechnol. 2019;18:29-75. DOI:10.1007/s11157-018-09491-9

Л.В. Маринченко[1]*, В.В. Хохлов[2], О.І.Ніжельська[3], В.О.Голуб[4]

[1]КПІ ім. Ігоря Сікорського, Київ, Україна
[2]Громадська організація «Аніль», Київ, Україна
[3]Інститут прикладної фізики НАН України, Суми, Україна
[4]Стокгольмський університет, Стокгольм, Швеція

ЗАСТОСУВАННЯ КОРЕЛЯЦІЙНОГО АНАЛІЗУ ЗОБРАЖЕНЬ ДЛЯ ВИЯВЛЕННЯ ЧУТЛИВОСТІ КЛІТИН ДО МАГНІТНОГО ПОЛЯ

Передумови. Підвищення техногенного електромагнітного навантаження залишає дискутивним питання його впливу на живі клітини, які не мають визначеного еволюційного механізму відповіді на такий екологічний чинник. Наразі недостатньо відповідних тестів, здатних виявляти вплив слабкого електромагнітного поля. Візуалізація морфологічних змін структури клітин простими оптичними методами не дає результату, отже додатковий механізм обробки зображень може бути корисним.
Мета. Перевірити придатність методу кореляційного аналізу мікрозображень на прикладі висохлих у фізрозчині дріжджових клітин на кремнієвій підкладці, для виявлення впливу статичного магнітного поля на структуру поверхні клітин, які не мають до нього визначених механізмів чутливості.
Методика реалізації. Цифрові мікрозображення крапель суспензії дріжджів у фізрозчині, висохлих на кремнієвих підкладках за впливу статичного магнітного поля 0,17 Тл та без поля, аналізували одним із фрактальних методів – визначали параметр кореляційної вимірності, який базувався на матриці значень яскравості пікселів.
Результати. Показано придатність методу кореляційного аналізу для визначення змін у структурі поверхні дріжджових клітин та кришталиків хлориду натрію за впливу статичного магнітного поля 0,17 Тл під час висихання дріжджової суспензії: показник кореляційної вимірності, який свідчив про варіативність структур, для дріжджових клітин збільшився, а для кришталиків NaCl – зменшився.
Висновки. У випадку кореляційної вимірності, на відміну від інших вимірностей, її обчислення здійснюється за значеннями яскравості, отже, враховуються й ті елементи зображення, що майже не розрізняються оком. Саме тому цей метод виявився чутливим до змін у структурі та рельєфі клітинної стінки дріжджів, висохлих за впливу статичного магнітного поля 0,17 Тл, зафіксувавши її ускладнення, а також засвідчив більш однорідну структуру утворених кристалів NaCl.
Ключові слова: обробка зображень; фрактальний аналіз; кореляційна вимірність; дріжджові клітини; кремній; хлорид натрію; кристалізація; магнітне поле; чутливість; мікроскопія; властивості поверхні; біотехнології.